Pharmacogn. Res., 2027; 19(2):656-666.
https://www.phcogres.com

Original Article

Polydatin Regulates Macrophage Polarization Via Activation of the SIRT1/HMGB1 Pathway: Bioinformatics and *in vitro* Validation

Ke Liu[1,#], Chunjiao Yang[2,#], Xuanyu Wang[2], Li Li[2], Xin Liu[1], Junying Ding[1,2,*]

[1]Beijing Key Laboratory of Innovative Research on the Removing Stasis and Detoxification Theory in Infectious Diseases, Beijing Hospital of Traditional Chinese Medicine, Beijing, CHINA.
[2]Clinical Laboratory, Beijing Hospital of Traditional Chinese Medicine, Beijing, CHINA.
#These authors contributed equally to this work.

ABSTRACT

Background: Traditional treatment strategies for bacterial pneumonia have primarily targeted pathogens. However, immune imbalance is increasingly recognized as a key pathogenic factor, and macrophages play a central role in maintaining immune homeostasis. **Materials and Methods:** Transcriptome data were obtained from the GEO database. Differentially Expressed Genes (DEGs) were identified and subjected to GO and KEGG enrichment analyses. A Protein-Protein Interaction (PPI) network was constructed and hub genes were identified. Macrophage polarization model was established with Lipopolysaccharide (LPS) *in vitro*. SIRT1 deacetylation activity was measured using an NAD+/NADH colorimetric assay. Nucleocytoplasmic localization of HMGB1 was assessed by Immuno Fluorescence (IF). The interaction between SIRT1 and HMGB1 was evaluated by Co-Immunoprecipitation (Co-IP). The expression of hub genes was evaluated using qPCR. **Results:** Ten hub genes (IL-6, IL-10, CCL2, CCL5, CXCL10, ISG15, DDX58, GBP1, GBP5 and TNF) were identified, and their mRNA expression levels in NR8383 cells were consistent with the bioinformatics analysis. Molecular docking studies also exhibited a strong binding affinity between Polydatin (PD) and target molecules. *In vitro* experiments, LPS inhibited the expression of SIRT1 and increased the expression of HMGB1 and TLR4, while PD reversed the effect of LPS. Additionally, PD significantly attenuated LPS-induced HMGB1 nucleocytoplasmic translocation. SIRT1 knockdown attenuated the effects of PD. **Conclusion:** PD promotes HMGB1 deacetylation via SIRT1, modulating its active release and nucleocytoplasmic translocation, which mediates macrophage M2 polarization and contributes to immune homeostasis restoration by regulating immune-related hub genes.

Keywords: HMGB1, Inflammation, Macrophage Polarization, Polydatin, SIRT1.

Correspondence:
Prof. Junying Ding
Beijing Key Laboratory of Innovative Research on the Removing Stasis and Detoxification Theory in Infectious Diseases, Beijing Hospital of Traditional Chinese Medicine, Beijing, CHINA.
Email: 18211197728@163.com

Received: 25-05-2026;
Revised: 03-07-2026;
Accepted: 15-10-2026.

INTRODUCTION

Based on our previous research results, it was found that in bacterial pneumonia, pathogenic microorganisms persistently activate the host immune system, resulting in immune cell dysfunction, aberrant inflammatory responses, and disruption of the balance between pro-inflammatory and anti-inflammatory processes (Edwards and Brockmann, 2025; Liu *et al*., 2025). These immunological disturbances frequently lead to severe clinical manifestations (Zhang *et al*., 2025), underscoring the critical need to modulate immune cell activity and restore immunological homeostasis in this disease context.

Macrophages serve as central regulators of tissue homeostasis, inflammatory modulation, and wound repair processes, playing an indispensable role in innate and adaptive immunity (Bijnen *et al*., 2025; Pickering *et al*., 2024; Simón-Codina *et al*., 2024). As primary coordinators of immune responses, macrophages demonstrate remarkable functional plasticity in response to microenvironmental cues, with their polarization state being particularly consequential during disease pathogenesis, progression, and resolution (Vishnyakova *et al*., 2024; Yu *et al*., 2024). The polarization of macrophages represents a dynamic and reversible process that can be pharmacologically modulated, exerting significant influence over the initiation, development, and regression of various immune-mediated inflammatory conditions (Li *et al*., 2022; Martins *et al*., 2024). The two primary polarization phenotypes-pro-inflammatory M1 and anti-inflammatory M2 macrophages-are essential for appropriate termination of inflammatory cascades and facilitation of tissue regeneration following injury. During bacterial pneumonia,

OPEN ACCESS
Manuscript TECHNOMEDIA

DOI: 10.5530/pres.20270134

Copyright Information :
Copyright Author (s) 2027 Distributed under Creative Commons CC-BY 4.0

Publishing Partner : Manuscript Technomedia. [www.mstechnomedia.com]

macrophages predominantly adopt the M1 phenotype, characterized by robust production of pro-inflammatory mediators including High Mobility Group Box 1 (HMGB1), Toll-Like Receptor 4 (TLR4), and Nuclear Factor Kappa B (NF-κB) (Hu *et al.*, 2024; Zhang *et al.*, 2025). This excessive M1 activation can instigate uncontrolled inflammatory cascades, potentially culminating in life-threatening complications such as sepsis, septic shock, and multiple organ dysfunction syndrome (Fujii and Osaki, 2023; Hou *et al.*, 2025). However, as pulmonary inflammation resolves, macrophages undergo phenotypic switching from M1 to M2 (Wang *et al.*, 2021), resulting in diminished expression and secretion of pro-inflammatory factors, thereby promoting inflammation resolution and tissue recovery. Consequently, understanding the dynamic regulation of macrophage polarization and maintaining its equilibrium represents a crucial avenue for elucidating disease regression mechanisms and developing novel therapeutic strategies.

Polydatin (PD), also referred to as resveratrol glycoside, constitutes a bioactive compound formed through the conjugation of resveratrol with glucose, which undergoes enzymatic conversion to resveratrol *in vivo* via glycosidase activity (Dai *et al.*, 2025). Sirtuin 1 (SIRT1), the primary endogenous target of resveratrol, has been demonstrated to be activated by PD, conferring protection against acute lung injury through suppression of the HMGB1/NF-κB pathway in experimental sepsis models (Lan *et al.*, 2017; Liu *et al.*, 2022). Besides, PD increased SIRT1 activity, inhibited the nucleocytoplasmic translocation of HMGB1 in renal Tubular Epithelial Cells (RTECs), attenuated RTEC apoptosis (Xu *et al.*, 2019). Through SIRT1 activation, PD exhibits therapeutic potential across diverse inflammatory conditions. The present investigation focuses on macrophage polarization as a mechanistic framework to identify PD's molecular targets in bacterial pneumonia, with the ultimate goal of providing clinically relevant insights for inflammatory diseases diagnosis and treatment.

MATERIALS AND METHODS

Data sources

The National Center for Biotechnology Information Gene Expression Omnibus (NCBI-GEO, https://www.ncbi.nlm.nih.gov/geo/) database was utilized as the primary source of gene expression profiles. Using the search term "Bacterial pneumonia" in the GEO with the species setting to "*Homo sapiens*," we obtained a transcriptomic dataset (GSE40885). The chip data contain 7 saline-instilled lung subsegment samples and 7 LPS-instilled lung subsegment samples. Targets associated with macrophage polarization were obtained from dataset GSE117040, using the keyword "Macrophage polarization". The GSE117040 dataset comprises 8 available samples and macrophages derived from whole blood of healthy blood donors, with the detection platform being GPL16791.

Identification of Differentially Expressed Genes (DEGs)

Differential expression analysis was performed using GEO2R, an interactive web tool designed for comparing two sample groups under identical experimental conditions. DEGs related to bacterial pneumonia and macrophage polarization were identified using screening criteria of $p<0.05$ and |log2 Fold Change (FC)| > 1. A volcano plot and heatmap were generated using the ggplot2 package in R, respectively, to visualize the DEGs results. The intersection of DEGs of two databases was determined using Venn diagrams (http://jvenn.toulouse.inra.fr/app/example.html). The detailed procedures can be seen in Figure 1A.

GO and KEGG enrichment analysis

Functional enrichment analysis was conducted using the Database for Annotation Visualization and Integrated Discovery (DAVID, https://david.ncifcrf.gov/). GO analysis encompassed three categories: Biological Process (BP), Molecular Function (MF), and Cellular Component (CC). KEGG pathway analysis was performed to identify significantly enriched pathways. A threshold of $p<0.05$ was set for statistical significance.

PPI network construction and hub genes analysis

DEGs were analyzed using the STRING database (https://cn.string-db.org/) with a confidence score cutoff >0.40 and restricted to *Homo sapiens*. The resulting Protein-Protein Interaction (PPI) network was visualized using Cytoscape software (version 3.9.1). Network topology parameters including degree, Maximal Clique Centrality (MCC), closeness, and betweenness were calculated to identify hub genes. The top 30 genes from each algorithm were intersected using Venn diagrams, with the overlapping genes designated as hub genes.

Molecular docking

The three-dimensional structure of PD was obtained from PubChem database and converted to Mol2 format using Open Babel software. Hydrogen atoms were added using UCSF Chimera software. Protein structures for target genes were retrieved from UniProt database and RCSB Protein Data Bank (all databases accessed November 2023). Molecular docking simulations were performed using SwissDock web server and results were visualized with UCSF Chimera.

Cell Culture and Drug Administration

NR8383 cells were procured in Procell (Wuhan, China) and were cultured in Ham's F-12K (Procell, China) supplemented with 20% Fetal Bovine Serum (FBS) (Gibco, USA) and 1% penicillin/streptomycin (P/S) (Gibco, USA). Cultures were maintained at 37°C in a humidified atmosphere containing 5% CO_2, passaged at 80% confluency. LPS (1 μg/mL, Beyotime, China) was used to induce NR8383 cell and SIRT1-knockdown NR8383 cell

polarization for 24 hr. To evaluate PD's anti-inflammatory effects, the cells were co-treated with 25 μg/mL PD for the indicated durations.

Construction of NR8383 cell with knockdown of SIRT1 gene

shRNA-SIRT1 and negative shRNA-control (shRNA-NC) were synthesized by He Yuan Biotechnology Co., Ltd. NR8383 cells were incubated in 6 well plates at density of 5×10^5 cells/well and cells were infected for 72 hr with either empty vector control (GL427NC2) or target viruses (Y30961 and Y31568), followed by selection with 2 μg/mL puromycin to eliminate non-transduced cells and establish stable knockdown cell lines. After transfection, the shRNA knockdown efficiency was identified using qRT-PCR and western blotting.

Immunofluorescence Staining

Cells were seeded at 5×10^4 cells/well in Matrigel-coated 24-well plates. Following treatments, cells were fixed with 4% Paraformaldehyde (PFA) for 20 min at Room Temperature (RT), permeabilized with PBS containing 0.1% Triton X-100 (PBS-T) for 10 min at RT, and blocked with 5% Bovine Serum Albumin (BSA) in PBS-T for 30 min at RT. Primary antibody incubation used HMGB1 polyclonal antibody (1:1500, Proteintech 10829-1-AP, Wuhan, China) followed by Alexa Fluor 488-labeled goat anti-rabbit IgG secondary antibody (1:500, Beyotime A0423, Shanghai, China).

RNA Isolation and Quantitative Real-Time PCR

Total RNA was extracted using Trizol reagent and reverse transcribed using Tiangen First Strand cDNA Synthesis Kit. Gene expression levels were quantified using the $2^{-\Delta\Delta Ct}$ method with Actin as an internal control.

Western blotting

Protein samples (20 μg per lane) were separated by 10% SDS-PAGE and transferred to Polyvinylidene Difluoride (PVDF) membranes. Membranes were blocked with 5% skim milk in Tris-buffered saline with Tween-20 (TBST) for 1 hr at RT, the membranes were incubated overnight at 4°C with primary antibodies: SIRT1 (1:1000, Abcam ab18239, Cambridge, UK), HMGB1(1:5000, Proteintech 10829-1-AP, Wuhan, China), TLR4 (1:1000, Proteintech 19811-1-AP, Wuhan, China) and Actin (1:5000, Proteintech 20536-1-AP, Wuhan, China) as the loading controls. Horseradish peroxidase-conjugated secondary antibodies were applied for 1 hr at RT. Protein bands were visualized using Enhanced Chemiluminescence (ECL) reagents (Thermo Scientific) and quantified using Image Lab software.

Statistical analysis

All statistical analyses were performed using GraphPad Prism 9.0 software. One-way ANOVA was used for multiple group comparisons. Data are presented as mean ± SD. A p-value <0.05 was considered statistically significant.

RESULTS

Identification of DEGs

The GSE40885 microarray was obtained from GEO to verify the DEGs in LPS and control groups in alveolar macrophages. Then, 522 DEGs were screened, including 453 up-regulated and 69 down-regulated genes (Figure 1B). Heatmap analysis demonstrated distinct expression patterns across samples, with red indicating high expression and blue indicating low expression, scaled according to |log 2FC| values. In the GSE117040 dataset, associated with macrophage polarization, we identified 2,685 DEGs, including 1,460 up-regulated and 1,225 down-regulated genes (Figure 1C). Venn diagram analysis identified 180 overlapping genes (Figure 1D) between bacterial pneumonia-related DEGs and macrophage polarization-related DEGs.

Functional enrichment analysis of intersecting DEGs

To better comprehend the different pathways and biological features of 180 intersecting DEGs, three GO categories: Biological Process (BP), Molecular Function (MF) and cellular com-ponent (CC) were analyzed using the DAVID database and yielded 171 significant terms, including 123 BP, 19 CC, and 29 MF terms. The top 10 most significant terms from each category were selected based on P-values and visualized in bubble plots, where bubble size corresponds to gene count and color intensity reflects p-value magnitude (Figure S1). GO_BP results revealed significant enrichment in inflammatory response, defense response to virus, and immune response. GO_MF results highlighted significant enrichment in chemokine activity, CCR chemokine receptor binding and cytokine activity. GO_CC results showed significant enrichment in extracellular space, region, and membrane. KEGG pathway analysis revealed that the 180 DEGs participated in 42 pathways, with 27 pathways meeting the significance threshold of $p<0.05$. The top 20 pathways were visualized in a bubble plot (Figure S1) using the same parameters as the GO analysis.

PPI network construction and hub genes identification

STRING database analysis of the intersecting DEGs generated a PPI network that was visualized using Cytoscape 3.9.1. Network topology analysis using four algorithms (MCC, Degree, Closeness, and Betweenness) identified hub genes, with the top 30 genes from each method selected for further analysis. Intersection of these gene sets yielded 10 core hub genes, including IL-6, IL-10, CCL2, CCL5, CXCL10, ISG15, DDX58, GBP1, GBP5 and TNF

(Figure 2A). Violin plots comparing gene expression between bacterial pneumonia samples (GSE40885) and normal controls demonstrated significantly elevated expression of TNF, IL-6, IL-10, CXCL10, CCL2, CCL5, ISG15, DDX58, GBP1, and GBP5 in diseased samples, while GBP1 showing decreased expression (Figure 2B). Pearson correlation analysis revealed strong positive correlations (r approaching 1) among most hub genes, while GBP1 exhibited negative correlation (r approaching -1) with other core genes (Figure 2C). All of these hub genes are key immune-related molecules that play diverse roles in inflammatory regulation. Through literature review (Wei *et al.*, 2022), the SIRT1-HMGB1 axis, in conjunction with other factors, thus has cytokine, chemokine, and growth factor activity, orchestrating the inflammatory and immune response in lung diseases. Thus, we further validated IL-6, IL-10, CCL2, CCL5, CXCL10, ISG15, DDX58, GBP1, GBP5, SIRT1, HMGB1 and TLR4 as key targets for subsequent experimental validation.

Molecular docking of hub genes with PD

Molecular docking simulations were performed between PD and protein structures of hub genes obtained from the Protein Data Bank (PDB IDs: IL-6 [1alu], IL-10 [1ilk], CCL2 [1dok], CCL5 [5coy], CXCL10 [1o80], ISG15 [3rt3], DDX58 [3zd7], GBP1 [1f5n], GBP5 [7e5a], SIRT1 [5btr], HMGB1, TLR4 [3fxi]). Binding energies below -4.25 kcal/mol indicated good binding affinity, while energies below -7 kcal/mol represented strong binding (Table 1). Besides CCL2 and CCL5, all other hub genes showed strong binding. Visualization of selected docking results is presented in Figure S2.

Validation of knockdown effect of SIRT1

Lentiviral transduction of NR8383 cells resulted in successful Green Fluorescent Protein (GFP) expression in both empty vector control groups (GL427NC2) and SIRT1 knockdown (Y30961 and Y31568) (Figure S3A). Quantitative analysis using qPCR and western blot confirmed significantly reduced SIRT1 mRNA and protein expression levels in sh-SIRT1 group compared to the untransfected control and empty vector control groups

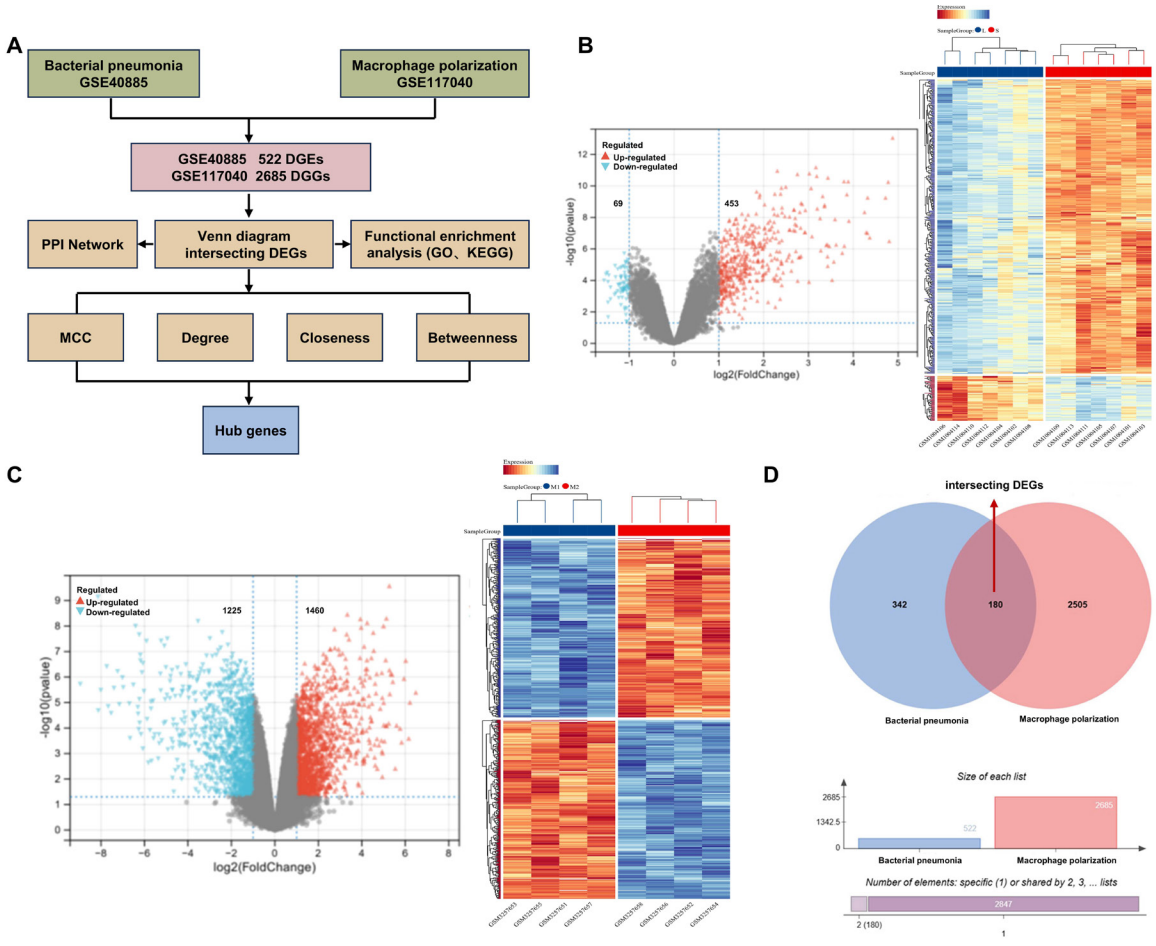


Figure 1: Identification of Differentially Expressed Genes (DEGs) from GEO datasets (GSE40885 and GSE117040). (A) Workflow for hub genes identification. (B) Volcano plot and heatmap of sifted-out DEGs in the GSE40885 dataset. (C) Volcano plot and heatmap of sifted-out DEGs in the GSE117040 dataset. (D) Venn diagram of the overlap of the genes between the two datasets. DEGs were defined using the criteria $|\log_2 FC|>1$ and $p<0.05$; upregulated genes are shown in red and downregulated genes in blue.

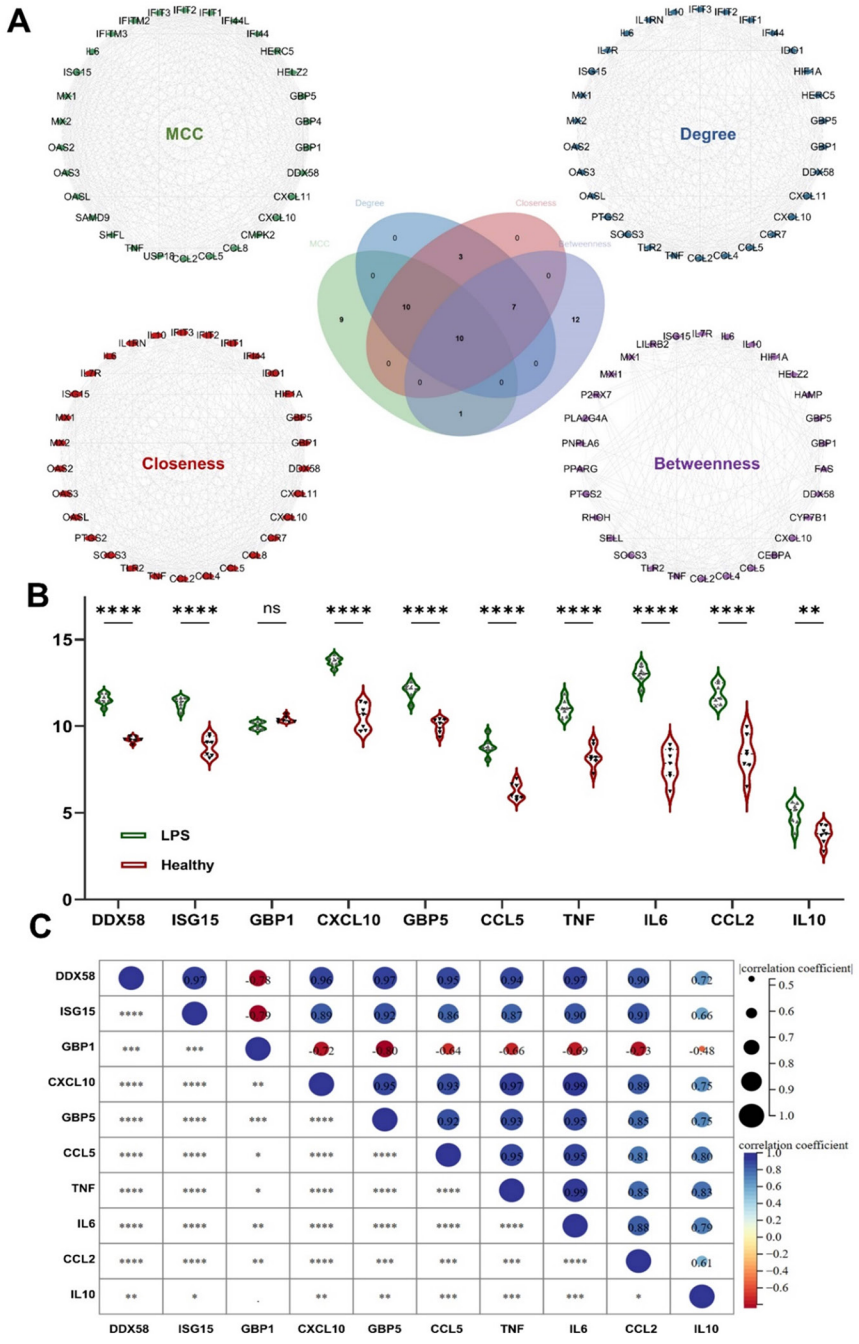


Figure 2: Identification of hub genes and their expression in control and bacterial pneumonia. (A) Screening the hub genes using the four topological measures: Betweeness, Closeness, Degree, and Maximal Clique Centrality (MCC) with the Analyze Network tool of the Cytoscape and 10 hub genes were identified. (B) Expression difference of ten hub genes between normal and bacterial pneumonia tissues. (C) Correlation analysis of ten hub genes, 0.3≤|r|≤0.5: low linear; 0.5≤|r|≤0.8: significant linear; |r|>0.8 high linear. *p<0.05; **p<0.01; ***p<0.001; ****p<0.0001; ns not significant.

(Figures S3B, S3C). Y31568 was used to construct stable SIRT1 knockdown NR8383 cell lines.

Bioinformatics prediction of HMGB1 deacetylation modification on SIRT1

PhosphoSitePlus (https://www.phosphosite.org/homeAction.action) database analysis predicted multiple acetylation sites on HMGB1 at residues 30, 44, 45, 55, 59, 82, 128, 157, and 172 (Figure S4A). Human Protein Atlas (HPA) database demonstrated high expression of HMGB1 in alveolar macrophages (Figure S4B) and the NoD web server showed between 79 and 99, 171 and 194 residue is the Nucleolar localization sequences (NoLSs) candidate segment region (Figure S4C). Subcellular localization analysis using Cell-PLoc 3.0 demonstrated HMGB1 may be localized in the nucleus, cytoplasm, and extracellular space (Figure S4D). HPA database further demonstrated HMGB1 expression

with both nuclear and cytoplasmic distribution (Figure S4E), suggesting potential nucleocytoplasmic translocation during macrophage activation, though further experimentation is required to confirm it.

PD promotes SIRT1 expression and deacetylation activity

LPS stimulation significantly decreased SIRT1 expression and NAD+/NADH ratio compared to control group ($p<0.05$). PD treatment reversed these effects ($p<0.05$), while SIRT1 knockdown abolished the protective effects of PD ($p<0.05$) (Figure 3A), indicating that PD enhances both SIRT1 expression and deacetylation activity.

PD inhibits HMGB1 expression and nucleocytoplasmic translocation

Co-immunoprecipitation experiments confirmed physical interaction between SIRT1 and HMGB1. LPS stimulation significantly increased HMGB1 and TLR4 expression compared to control ($p<0.05$), which was attenuated by PD treatment ($p<0.05$). SIRT1 knockdown prevented PD-mediated reduction of HMGB1 and TLR4 expression ($p<0.05$) (Figures 3B, 3C). Immunofluorescence analysis revealed LPS-induced translocation of HMGB1 from nucleus to cytoplasm, which was inhibited by PD treatment. This protective effect of PD was abolished in SIRT1 knockdown cells (Figure 4), demonstrating that PD regulates HMGB1 nucleocytoplasmic translocation through SIRT1.

PD regulates hub gene expression

qPCR analysis demonstrated that LPS stimulation significantly up-regulated DDX58, IL-6, CCL2, CCL5, CXCL10, ISG15, GBP1, and GBP5 expression while down-regulating IL-10 compared to control ($p<0.05$). PD treatment reversed these LPS-induced changes ($p<0.05$) other than ISG15 ($p>0.05$). In SIRT1 knockdown cells, the regulatory effects of PD on IL-6, IL-10, CCL5, CXCL10, GBP5, and DDX58 expression were significantly attenuated ($p<0.05$), while its effects on CCL2 and GBP1 expression were maintained ($p>0.05$) (Figure S5).

DISCUSSION

Macrophages serve as central regulators of immune responses, with M1 polarization playing a critical role in driving inflammatory processes during disease pathogenesis (Li *et al.*, 2022; Liu *et al.*, 2023; Zimmermann *et al.*, 2024). Our study demonstrates that LPS stimulation activates the canonical inflammatory pathway through binding to TLR4 on macrophage surfaces, triggering downstream signaling cascades and pro-inflammatory mediator release, including IL-6, CCL2, CXCL10 and DDX58 associated with M1-polarized macrophages. Using an LPS-stimulated NR8383 macrophage model, we investigated how PD modulates HMGB1 expression and related inflammatory pathways through SIRT1-mediated deacetylation. Our findings reveal that PD influences the HMGB1/TLR4 signaling pathway via SIRT1 activation, thereby regulating the immune microenvironment in LPS-induced inflammation. Notably, SIRT1 knockdown enhanced HMGB1 nucleocytoplasmic translocation and acetylation, activating TLR4 pathway signaling and counteracting PD's immunomodulatory effects. These results underscore SIRT1's pivotal role in mediating PD's effects on HMGB1 and downstream TLR4 signaling.

SIRT1, an evolutionarily conserved NAD+-dependent deacetylase belonging to the sirtuin family, regulates inflammation through HMGB1 deacetylation (Liu *et al.*, 2024; Shen *et al.*, 2025). Previous studies demonstrate that resveratrol inhibits HMGB1/TLR4/MyD88/NF-κB signaling via SIRT1 activation, attenuating neuroinflammatory responses and protecting against neonatal brain injury effects abolished by EX527 pretreatment (Le *et al.*, 2019). Paeonol deacetylated HMGB1 by upregulating SIRT1 level and SIRT1 inhibition rescued the paeonol-induced inhibition in inflammatory response (Liu *et al.*, 2024). Emodin alleviated oxidative stress, complement system activation, inflammation, and kidney injury in urosepsis rats through the AMPK/SIRT1 signaling pathway (Cui *et al.*, 2024). Salidroside increased the levels of SIRT1 expression but markedly reduced the phosphorylation of NF-κB and the expressions of NLRP3, cleaved caspase-1, and gasdermin D (GSDMD) induced by LPS (Meng *et al.*, 2024). In our study, PD intervention significantly increased SIRT1 protein expression, while SIRT1 knockdown markedly reduced expression levels. These findings align with

Table 1: Molecular docking results of PD and hub genes.

Gene name	Binding Energy (kcal/mol)	Gene name	Binding Energy (kcal/mol)
IL-6	-7.1	IL-10	-7.3
CXCL10	-7.2	CCL2	-6.8
CCL5	-6.5	ISG15	-7.0
DDX58	-7.5	GBP1	-7.6
GBP5	-8.3	SIRT1	-8.6
HMGB1	-7.9	TLR4	-8.6

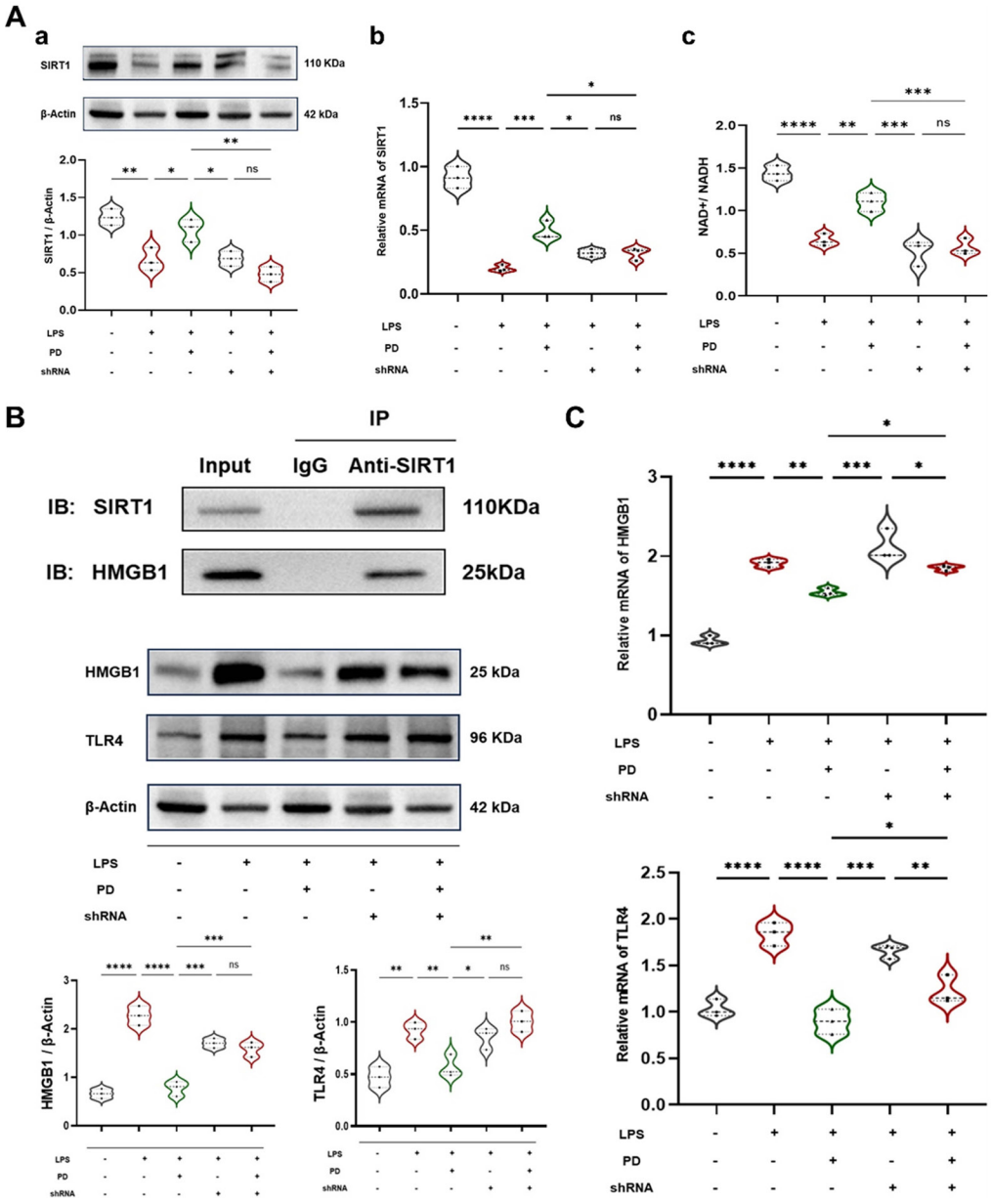


Figure 3: PD inhibits LPS-induced SIRT1-mediated changes in the expression of HMGB1 and TLR4. (A) the SIRT1 expression in protein (a), mRNA level (b) and deacetylation activity (c) in five groups. (B) Interaction between SIRT1 and HMGB1 was assayed by immunoprecipitation with anti-SIRT1 antibody and probed for co-precipitation of HMGB1 with SIRT1. The protein expression of HMGB1 and TLR4 were measured by western blot. (C) the mRNA level of HMGB1 and TLR4 in five groups. All data are expressed as mean values ± SD; *p<0.05, **p<0.01, ***p<0.001, ****p<0.0001, ns not significant.

existing literature and further establish SIRT1 as a key mediator of PD's anti-inflammatory actions.

HMGB1 functions as a non-histone nuclear protein with location-dependent activities. Intranuclear HMGB1 serves as a DNA chaperone maintaining chromosomal structure and function (Lee *et al.*, 2021), while extracellular HMGB1 acts as a damage-associated molecular pattern (DAMP) molecule that engages TLR4 and other pattern recognition receptors to regulate inflammation and immune homeostasis (Irzan *et al.*, 2025; Xiao *et al.*, 2025). HMGB1 secretion and release are precisely controlled through multiple mechanisms including post-translational modifications (acetylation, phosphorylation, methylation) (Chen *et al.*, 2022; Lenka *et al.*, 2018; Richard *et al.*, 2017) and cell death pathways (apoptosis, pyroptosis, necroptosis, ferroptosis) (Bai *et al.*, 2025; Li *et al.*, 2025; Zhao *et al.*, 2024). Consequently, HMGB1 and TLR4 represent important biomarkers and therapeutic targets for immune-mediated disorders. Our data also support previous findings and suggest HMGB1 levels are significantly elevated in inflammatory diseases. PD intervention can relieve this condition by activating SIRT1. Additionally, HMGB1 nucleocytoplasmic

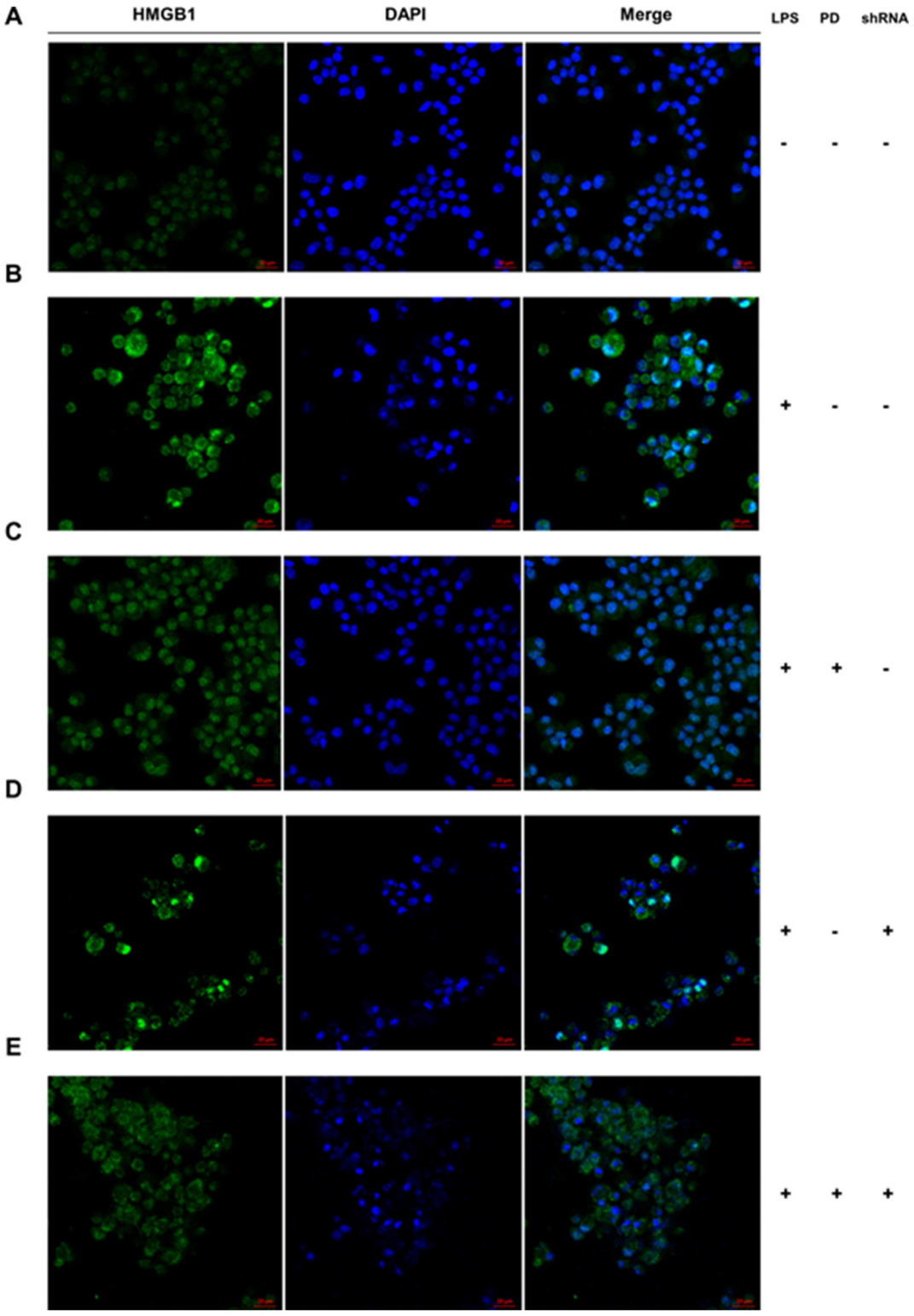


Figure 4: PD inhibits HMGB1 nucleocytoplasmic translocation through SIRT1. (A) Representative IF images of HMGB1 (green) localization in NR8383 cells were exam-ined with confocal microscope (Scale bar, 10 μm). Nucleus was indicated by DAPI (blue) staining. In control, HMGB1 stayed in the nucleus. (B) Compared to the control group, HMGB1 was relocated in the cytoplasm of the LPS-treated group. (C) After PD inter-vention, extranuclear HMGB1 expression decreased. PD inhibits HMGB1 nucleocyto-plasmic translocation. (D-E) When SIRT1 knockdown, there was still a tendency for HMGB1 to translocate to the extranuclear area regardless of PD.

translocation was suppressed. Therefore, PD may act as an anti-inflammatory agent via the SIRT1-HMGB1 axis.

The cytokines Interleukin-6 (IL-6) and Interleukin-10 (IL-10) serve as master regulators of inflammatory responses and immune homeostasis. IL-6 mediates inflammatory responses and immune regulation through IL-6 receptor activation, promoting immune cell activation and inflammatory mediator release that drives pulmonary inflammation and tissue injury (Barrett, 2024; Cao *et al*., 2024; Liu *et al*., 2025; Paranga *et al*., 2024; Sayed *et al*., 2025; Tsai *et al*., 2025). Conversely, IL-10 functions as a negative regulator that prevents immune hyperactivation, reduces inflammatory mediator production, and maintains immune balance during infections (Anh *et al*., 2025; Pan *et al*., 2025; Zhang *et al*., 2025). Previous studies show that hesperidin and Xuanfei Baidu decoction inhibit IL-6/STAT3 signaling, thus ameliorating bleomycin-induced pulmonary fibrosis and improving survival in murine models (Han *et al*., 2023; Wang *et al*., 2022). In LPS-induced acute lung injury models, IL-10 signaling blockade impairs macrophage activation and recruitment while increasing pro-inflammatory factor expression and leukocyte infiltration, exacerbating lung injury (Nie *et al*., 2024). Our study demonstrates that PD intervention significantly reduces IL-6 secretion while increasing IL-10 release. SIRT1 knockdown reversed these immunomodulatory effects, indicating that PD suppresses LPS-induced inflammation through SIRT1-dependent mechanisms.

Chemokine family members C-X-C Motif Chemokine Ligand 10 (CXCL10), C-C motif Chemokine Ligand 2 (CCL2), and CCL5 play crucial roles in immune cell migration, activation, and differentiation. CXCL10, produced by monocytes, macrophages, dendritic cells, and T cells, recruits and activates CD4+ T cells, CD8+ T cells, and Natural Killer (NK) cells during antiviral and antitumor immune responses (Lin *et al*., 2024; Makuch *et al*., 2022; Xia *et al*., 2021). CCL2 (monocyte chemoattractant protein-1), secreted by macrophages, dendritic cells, and fibroblasts, attracts monocytes, memory T cells, and dendritic cells to inflammatory sites (Lin *et al*., 2022). CCL5, produced by macrophages, dendritic cells, and T cells, exhibits potent chemotactic activity toward lymphocytes and monocytes (Kwankaew *et al*., 2024). Studies in influenza A virus-infected mice demonstrate that combined oseltamivir and etanercept treatment downregulates inflammatory cytokines (TNF, IL-1β, IL-6) and chemokines (CCL2, CCL5, CXCL10), suggesting therapeutic potential for pneumonia management (Pandey *et al*., 2023). In our study, PD intervention significantly reduced the LPS-induced expression of IL6, CCL2, CCL5, and CXCL10 ($p<0.05$), and increased the expression of IL-10, which have been reported to be associated with M1/M2 polarization (Tsai *et al*., 2021).

Several limitations warrant consideration in this study. First, LPS derived from Gram-negative bacterial cell walls may not fully recapitulate intact Gram-negative bacterial infections or account for Gram-positive bacterial pathogenesis. Second, macrophage responses to LPS may differ from neutrophil-dominated immune responses characteristic of clinical bacterial infections. Third, the precise *in vivo* mechanisms of PD's effects in inflammatory diseases remain unclear and require further investigation-a key focus for our ongoing research. Future studies should address these limitations through comprehensive *in vivo* models and clinical translational research.

CONCLUSION

The macrophages polarization is a decisive factor for the development of inflammatory diseases. Our research results indicated that PD can regulate the polarization balance of macrophages through the SIRT1/HMGB1 axis, to effectively prevent and treat inflammatory diseases. PD is a promising candidate for the prevention and treatment of inflammatory diseases.

ACKNOWLEDGEMENT

This work was supported by the Beijing Construction Program for High-level Public Health of Technical Talents [2022-3-009].

ABBREVIATIONS

BP: Biological Process; **CC:** Cell Component; **Co-IP:** Co-immunoprecipitation; **CXCL:** C-X-C Motif Chemokine Ligand; **DAVID:** Database for Annotation, Visualization and Integrated Discovery; **DDX58:** Retinoic acid-inducible gene I; **DEGs:** Differentially expressed genes; **FC:** Fold change; **GBP:** Guanylate binding protein; **GEO:** Gene Expression Omnibus; **GO:** Gene Ontology; **HMGB1:** High Mobility Group Box-1; **IF:** Immunofluorescence; **IL-1β:** Interleukin-1β; **IL-6:** Interleukin-6; **IL-10:** Interleukin-10; **ISG15:** Interferon-stimulated gene 15; **KEGG:** Kyoto Encyclopedia of Genes and Genomes; **LPS:** Lipopolysaccharide; **MF:** Molecular Function; **NAD+:** Nicotinamide adenine dinucleotide; **NADH:** Reduced nicotinamide adenine dinucleotide; **NF-κB:** Nuclear Factor-κb; **NoLSs:** Nucleolar localization sequences; **PD:** Polydatin; **PPI:** Protein-Protein Interaction; **qPCR:** Quantitative Real-time PCR; **shRNA:** Short hairpin RNA; **SIRT1:** Silent Information Regulator 1; **TLR4:** Toll-Like Receptor 4; **TNF:** Tumor necrosis factor.

CONFLICT OF INTEREST

The authors declare that there is no conflict of interest.

ETHICAL STATEMENT

This study utilized the NR8383 cell line (rat alveolar macrophages) and publically available transcriptomic data from the NCBI-GEO database (GSE40885 and GSE117040). All experimental procedures were conducted in accordance with the institutional guidelines for laboratory animal cell culture and data usage.

SUMMARY

This study identifies the molecular mechanism by which Polydatin (PD) modulates immune homeostasis in bacterial pneumonia. Through bioinformatics and *in vitro* validation, it was found that PD activates SIRT1, which promotes the deacetylation of HMGB1. This process inhibits the nucleocytoplasmic translocation of HMGB1 and suppresses the TLR4 signaling pathway, effectively shifting macrophages from a pro-inflammatory M1 phenotype to an anti-inflammatory M2 phenotype.

REFERENCES

Anh, D. D., Vugrek, L., The, N. T., Hafza, N., My, T. N., Linh, L. T. K., *et al.* (2025). Characterization of dengue patients in Vietnam: Clinical, virological, and IL-10 profiles during 2021- 2022 outbreaks. PLoS Negl Trop Dis, 19(3), e0012954. https://doi.org/10.1371/journal.pntd.0012954

Bai, T., Guo, H. L., Wang, F., Kang, Y. Y., Zhang, H. T., Dong, L., & Yang, Y. (2025). Gut microbiota and HMGB1/NLRP3/GSDMD inflammasome-dependent pyroptosis: Mechanisms by physcion ameliorates alcoholic liver fibrosis. Front Pharmacol, 16, 1532590. https://doi.org/10.3389/fphar.2025.1532590

Barrett, D. (2024). IL-6 blockade in cytokine storm syndromes. Adv Exp Med Biol, 1448, 565–572. https://doi.org/10.1007/978-3-031-59815-9_37

Bijnen, M., Sridhar, S., Keller, A., & Greter, M. (2025). Brain macrophages in vascular health and dysfunction. Trends Immunol, 46(1), 46-60. https://doi.org/10.1016/j.it.2024.11.012

Cao, L., Lin, M., Sheng, F., Chen, B., & Hu, C. (2024). Efficacy and inflammatory levels (IL-6, IL-10) of adjuvant application of vitamin-A in the treatment of pediatric Mycoplasma pneumoniae pneumonia: A systematic review and meta-analysis. Front Pediatr, 12, 1345458. https://doi.org/10.3389/fped.2024.1345458

Chen, R., Kang, R., & Tang, D. (2022). The mechanism of HMGB1 secretion and release. Exp Mol Med, 54(2), 91-102. https://doi.org/10.1038/s12276-022-00736-w

Cui, J., Wang, S., Bi, S., Zhou, H., & Sun, L. (2024). Emodin-based regulation and control of serum complement C5a, oxidative stress, and inflammatory responses in rats with urosepsis via AMPK/SIRT1. Iran J Allergy Asthma Immunol, 23(5), 550-562. https://doi.org/10.18502/ijaai.v23i5.16750

Dai, J., Yan, Z., Zhao, K., Li, X., Zang, Y., Xu, Q., & Zhu, F. (2025). Efficient synthesis of polydatin by a two-enzyme coupled with one-pot method. Sheng Wu Gong Cheng Xue Bao, 41(1), 461-473. https://doi.org/10.13345/j.cjb.240398

Edwards, M., & Brockmann, L. (2025). Microbiota-dependent modulation of intestinal anti-inflammatory CD4(+) T cell responses. Semin Immunopathol, 47(1), 23. https://doi.org/10.1007/s00281-025-01049-6

Fujii, J., & Osaki, T. (2023). Involvement of nitric oxide in protecting against radical species and autoregulation of M1-Polarized macrophages through metabolic remodeling. Molecules, 28(2). https://doi.org/10.3390/molecules28020814

Han, D., Gong, H., Wei, Y., Xu, Y., Zhou, X., Wang, Z., & Feng, F. (2023). Hesperidin inhibits lung fibroblast senescence via IL-6/STAT3 signaling pathway to suppress pulmonary fibrosis. Phytomedicine, 112, 154680. https://doi.org/10.1016/j.phymed.2023.15468

Hou, F. F., Mi, J. H., Wang, Q., Tao, Y. L., Guo, S. B., Ran, G. H., & Wang, J. C. (2025). Macrophage polarization in sepsis: Emerging role and clinical application prospect. Int Immunopharmacol, 144, 113715. https://doi.org/10.1016/j.intimp.2024.113715

Hu, M., Jin, F., Zhang, C., Shao, J., Wang, C., Wang, T., & Wu, D. (2024). Sodium houttuyfonate induces bacterial lipopolysaccharide shedding to promote macrophage M1 polarization against acute bacterial lung infection. Biomed Pharmacother, 179, 117358. https://doi.org/10.1016/j.biopha.2024.117358

Irzan, F. I., Retinasamy, T., Wen, W. R., Sheng, E. T. M., Shaikh, M. F., & Arulsamy, A. (2025). The Role of HMGB1 in infection-related cognitive deficits. Front Biosci (Landmark Ed), 30(2), 25544. https://doi.org/10.31083/fbl25544

Kwankaew, P., Mahittikorn, A., Mala, W., Kotepui, K. U., Anabire, N. G., Wilairatana, P., & Kotepui, M. (2024). Association between RANTES/CCL5 levels with Plasmodium infections and malaria severity: a systematic review. Malar J, 23(1), 335. https://doi.org/10.1186/s12936-024-05152-1

Lan, K. C., Chao, S. C., Wu, H. Y., Chiang, C. L., Wang, C. C., Liu, S. H., & Weng, T. I. (2017). Salidroside ameliorates sepsis-induced acute lung injury and mortality via downregulating NF-κB and HMGB1 pathways through the upregulation of SIRT1. Sci Rep, 7(1), 12026. https://doi.org/10.1038/s41598-017-12285-8

Le, K., Chibaatar Daliv, E., Wu, S., Qian, F., Ali, A. I., Yu, D., & Guo, Y. (2019). SIRT1-regulated HMGB1 release is partially involved in TLR4 signal transduction: A possible anti-neuroinflammatory mechanism of resveratrol in neonatal hypoxic-ischemic brain injury. Int Immunopharmacol, 75, 105779. https://doi.org/10.1016/j.intimp.2019.105779

Lee, J. H., Song, W. J., An, J. H., Chae, H. K., Park, S. M., Li, Q., & Youn, H. Y. (2021). Role of serum high-motility group box-1 (HMGB1) concentration as a prognostic factor in canine acute pancreatitis: A pilot study. Res Vet Sci, 141, 26–32. https://doi.org/10.1016/j.rvsc.2021.09.013

Lenka, S. S., Paichha, M., Basu, M., & Samanta, M. (2018). LrHMGB1 shares structural similarities with human HMGB1, and its expression is induced in bacterial Infection, antiviral vaccination, and pathogen-associated molecular patterns stimulation. DNA Cell Biol, 37(8), 708-723. https://doi.org/10.1089/dna.2018.4221

Li, Q. R., Tan, S. R., Yang, L., He, W., Chen, L., Shen, F. X., Wang, Z., & Wang, H. F. (2022). Mechanism of chlorogenic acid in alveolar macrophage polarization in Klebsiella pneumoniae-induced pneumonia. J Leukoc Biol, 112(1), 9-21. https://doi.org/10.1002/jlb.3hi0721-368r

Li, S., Wang, Y., Wu, M., Younis, M. H., Olson, A. P., Barnhart, T. E., *et al.* (2022). Spleen-targeted glabridin-loaded nanoparticles regulate polarization of Monocyte/Macrophage (M(o) /M(φ)) for the treatment of cerebral ischemia-reperfusion injury. Adv Mater, 34(39), e2204976. https://doi.org/10.1002/adma.202204976

Li, Y., Gao, X., Chen, Y., Li, H., Tang, J., & Sun, W. (2025). Independent and interactive roles of hirudin and HMGB1 interference in protecting renal function by regulating autophagy, apoptosis, and kidney injury in chronic kidney disease. Eur J Histochem, 69(2), 4182. https://doi.org/10.4081/ejh.2025.4182

Lin, J. B., Pepple, K. L., Concepcion, C., Korshunova, Y., Paley, M. A., Paley, G. L., *et al.* (2024). Aqueous macrophages contribute to conserved CCL2 and CXCL10 gradients in uveitis. Ophthalmol Sci, 4(4), 100453. https://doi.org/10.1016/j.xops.2023.100453

Lin, Z., Shi, J. L., Chen, M., Zheng, Z. M., Li, M. Q., & Shao, J. (2023). CCL2: An important cytokine in normal and pathological pregnancies: A review. Front Immunol, 13, 1053457. https://doi.org/10.3389/fimmu.2022.1053457

Liu, F. J., Gu, T. J., & Wei, D. Y. (2022). Emodin alleviates sepsis-mediated lung injury via inhibition and reduction of NF-kB and HMGB1 pathways mediated by SIRT1. Kaohsiung J Med Sci, 38(3), 253-260. https://doi.org/10.1002/kjm2.12476

Liu, H., Yang, R., Zhao, S., Zhou, F., Liu, Y., Zhou, Z., Chen, L., & Xie, J. (2023). Collagen scaffolds derived from bovine skin loaded with MSC optimized M1 macrophages remodeling and chronic diabetic wounds healing. Bioeng Transl Med, 8(3), e10467. https://doi.org/10.1002/btm2.10467

Liu, Y., Xu, T., Tan, Q., & Xiong, L. (2025). Effects of Candida colonization on patients with ventilator-associated pneumonia and pathogenic microorganisms: Systematic review and meta-analysis. Diagn Microbiol Infect Dis, 111(1), 116580. https://doi.org/10.1016/j.diagmicrobio.2024.116580

Liu, Z., Ou, Y., He, X., Yuan, T., Li, M., Long, Y., Li, Y., & Tan, Y. (2025). Guardians of the lung: the multifaceted roles of macrophages in cancer and infectious disease. DNA Cell Biol, 44(6), 249-262. https://doi.org/10.1089/dna.2024.0211

Liu, Z., Zhu, J., Pan, E., Pang, L., Zhou, X., & Che, Y. (2024). Paeonol alleviates subarachnoid hemorrhage injury in rats through upregulation of SIRT1 and inhibition of HMGB1/TLR4/MyD88/NF-κB pathway. J Biochem Mol Toxicol, 38(12), e70035. https://doi.org/10.1002/jbt.70035

Makuch, E., Jasyk, I., Kula, A., Lipiński, T., & Siednienko, J. (2022). IFNβ-induced CXCL10 chemokine expression is regulated by pellino3 ligase in monocytes and macrophages. Int J Mol Sci, 23(23), 14915. https://doi.org/10.3390/ijms232314915

Martins, R. A., Costa, F. R., Pires, L., Santos, M., Santos, G. S., Lana, J. V., *et al.* (2024). Regenerative inflammation: The mechanism explained from the perspective of buffy-coat protagonism and macrophage polarization. Int J Mol Sci, 25(20), 11329. https://doi.org/10.3390/ijms252011329

Meng, J., Li, Y., Sun, F., Feng, W., Ye, H., Tian, T., & Lei, M. (2024). Salidroside alleviates LPS-induced liver injury and inflammation through SIRT1- NF-κB pathway and NLRP3 inflammasome. Iran J Basic Med Sci, 27(3), 297-303. https://doi.org/10.22038/ijbms.2023.69401.15124

Nie, Z., Fan, Q., Jiang, W., Wei, S., Luo, R., Hu, H., Liu, G., Lei, Y., & Xie, S. (2024). Placental mesenchymal stem cells suppress inflammation and promote M2-like macrophage polarization through the IL-10/STAT3/NLRP3 axis in acute lung injury. Front Immunol, 15, 1422355. https://doi.org/10.3389/fimmu.2024.1422355

Pan, X., Huang, Z., Tao, N., Huang, C., Wang, S., Cheng, Z., Fan, R., & Liu, S. (2025). Increased circulating levels of SP-D and IL-10 are associated with the development of disease severity and pulmonary fibrosis in patients with COVID-19. Front Immunol, 16, 1553283. https://doi.org/10.3389/fimmu.2025.1553283

Pandey, P., Al Rumaih, Z., Kels, M. J. T., Ng, E., Kc, R., Malley, R., Chaudhri, G., & Karupiah, G. (2023). Therapeutic targeting of inflammation and virus simultaneously ameliorates influenza pneumonia and protects from porbidity and portality. Viruses, 15(2), 318. https://doi.org/10.3390/v15020318

Paranga, T. G., Mitu, I., Pavel-Tanasa, M., Rosu, M. F., Miftode, I. L., Constantinescu, D., *et al.* (2024). Cytokine storm in COVID-19: Exploring IL-6 signaling and cytokine-microbiome interactions as emerging therapeutic approaches. Int J Mol Sci, 25(21), 11411. https://doi.org/10.3390/ijms252111411

Pickering, S., Wilson, H., Bravo, E., Perera, M. R., Seow, J., Graham, C., *et al.* (2024). Antibodies to the RBD of SARS-CoV-2 spike mediate productive infection of primary human macrophages. Nat Commun, 15(1), 10764. https://doi.org/10.1038/s41467-024-54458-w

Richard, S. A., Jiang, Y., Xiang, L. H., Zhou, S., Wang, J., Su, Z., & Xu, H. (2017). Post-translational modifications of high mobility group box 1 and cancer. Am J Transl Res, 9(12), 5181-5196.

Sayed, A. E., Hafez, A., Ateya, A., Darwish, A., & Tahoun, A. (2025). Single nucleotide polymorphisms, gene expression and evaluation of immunological, antioxidant, and pathological parameters associated with bacterial pneumonia in Barki sheep. Ir Vet J, 78(1), 11. https://doi.org/10.1186/s13620-025-00296-1

Shen, P., Lin, W., Huang, Y., Ba, X., Han, L., Li, T., Qin, K., Chen, Z., & Tu, S. (2025). Wutou decoction attenuates rheumatoid arthritis in rats through SIRT1-mediated deacetylation of the HMGB1/NF-κB pathway. J Ethnopharmacol, 337(Pt 3), 118921. https://doi.org/10.1016/j.jep.2024.118921

Simón-Codina, B., Cacho-Pujol, J., Moles, A., & Melgar-Lesmes, P. (2024). Reprogramming macrophages to treat liver diseases. Hepatology. 84(1), 251. https ://doi.org/10.1097/hep.0000000000001160

Tsai, C. F., Chen, G. W., Chen, Y. C., Shen, C. K., Lu, D. Y., Yang, L. Y., Chen, J. H., & Yeh, W. L. (2021). Regulatory effects of quercetin on M1/M2 macrophage polarization and oxidative/antioxidative balance. Nutrients, 14(1), 67. https://doi.org/10.3390/nu140 10067

Tsai, Y. H., Hung, K. Y., & Fang, W. F. (2025). Leptin and Iinterlukin-6 relationship and influence of mortality in sepsis. BMC Infect Dis, 25(1), 460. https://doi.org/10.1186/ s12879-025-10829-2

Vishnyakova, P., Gantsova, E., Kiseleva, V., Lazarev, D., Knyazev, E., Poltavets, A., Iskusnykh, M., Muminova, K., Potapova, A., Khodzhaeva, Z., Elchaninov, A., Fatkhudinov, T., & Sukhikh, G. (2024). MicroRNA miR-27a as a possible regulator of anti-inflammatory macrophage phenotype in preeclamptic placenta. Placenta, 145, 151–161. https:// doi.org/10.1016/j.placenta.2023.12.003

Wang, X., Ji, Y., Feng, P., Liu, R., Li, G., Zheng, J., *et al.* (2021). The m6A reader IGF2BP2 regulates macrophage phenotypic activation and inflammatory diseases by stabilizing TSC1 and PPARγ. Adv Sci (Weinh), 8(13), 2100209. https://doi.org/10.10 02/advs.202100209

Wang, Y., Sang, X., Shao, R., Qin, H., Chen, X., Xue, Z., Li, L., Wang, Y., Zhu, Y., Chang, Y., Gao, X., Zhang, B., Zhang, H., & Yang, J. (2022). Xuanfei Baidu Decoction protects against macrophages induced inflammation and pulmonary fibrosis via inhibiting IL-6/ STAT3 signaling pathway. J Ethnopharmacol, 283, 114701. https://doi.org/10.1016/j. jep.2021.114701

Wei, L., Zhang, W., Li, Y., & Zhai, J. (2022). The SIRT1-HMGB1 axis: Therapeutic potential to ameliorate inflammatory responses and tumor occurrence. Front Cell Dev Biol, 10, 986511. https://doi.org/10.3389/fcell.2022.986511

Xia, M., Chen, J., Meng, G., Shen, H., & Dong, J. (2021). CXCL10 encoding synNotch T cells enhance anti-tumor immune responses without systemic side effect. Biochem Biophys Res Commun, 534, 765–772. https://doi.org/10.1016/j.bbrc.2020.11.002

Xiao, Y., Hao, L., Cao, X., Zhang, Y., Xu, Q., Qin, L., *et al.* (2025). Interleukin-33 knockout promotes High Mobility Group Box 1 release from astrocytes by acetylation mediated by P300/CBP-associated factor in experimental autoimmune encephalomyelitis. Neurosci Bull, 41(7), 1181-1197. https://doi.org/10.1007/s12264-025-01374-8

Xu, S., Zeng, Z., Zhao, M., Huang, Q., Gao, Y., Dai, X., *et al.* (2019). Evidence for SIRT1 mediated HMGB1 release from kidney cells in the early stages of hemorrhagic shock. Front Physiol, 10, 854. https://doi.org/10.3389/fphys.2019.00854

Yu, C., Zhang, C., Huai, Y., Liu, D., Zhang, M., Wang, H., Zhao, X., Bo, R., Li, J., & Liu, M. (2024). The inhibition effect of caffeic acid on NOX/ROS-dependent macrophages M1-like polarization contributes to relieve the LPS-induced mice mastitis. Cytokine, 174, 156471. https://doi.org/10.1016/j.cyto.2023.156471

Zhang, J., Lv, T., Tan, S., Yu, L., Chi, Y., Chen, J., Fan, X., & Lu, X. (2025). Screening helper T lymphocyte epitopes based on IFN-γ/IL-10 ratio for developing a novel multi-epitope vaccine candidate using Wolbachia surface protein as an adjuvant against visceral leishmaniasis. Parasit Vectors, 18(1), 116. https://doi.org/10.1186/ s13071-025-06756-5

Zhang, M., Jia, H., Zhuang, L., Xu, Y., Zhang, T., Gu, J., He, S., & Li, D. (2025). Ultrathin high-entropy hydrotalcites-based injectable hydrogel with programmed bactericidal and anti-inflammatory effects to accelerate drug-resistant bacterial infected wound healing. Colloids Surf B Biointerfaces, 247, 114450. https://doi.org/10.1016/j. colsurfb.2024.114450

Zhang, R., Zuo, Y., & Li, S. (2025). Mycoplasma pneumoniae MPN606 induces inflammation by activating MAPK and NF-κB signaling pathways. Microb Pathog, 200, 107288. https://doi.org/10.1016/j.micpath.2025.107288

Zhao, G., Wang, X., Lei, H., Ruan, N., Yuan, B., Tang, S., Ni, N., Zuo, Z., Xun, L., Luo, M., Zhao, Q., Qi, J., & Fu, P. (2024). Serum HMGB-1 released by ferroptosis and necroptosis as a novel potential biomarker for systemic lupus erythematosus. Int Immunopharmacol, 140, 112886. https://doi.org/10.1016/j.intimp.2024.112886

Zimmermann, J. A., Lucht, K., Stecher, M., Badhan, C., Glaser, K. M., Epple, M. W., *et al.* (2024). Functional multi-organelle units control inflammatory lipid metabolism of macrophages. Nat Cell Biol, 26(8), 1261-1273. https://doi.org/10.1038/s41556-024 -01457-0.

Cite this article: Liu K, Yang C, Wang X, Li L, Liu X, Ding J. Polydatin Regulates Macrophage Polarization Via Activation of the SIRT1/HMGB1 Pathway: Bioinformatics and *in vitro* Validation. Pharmacog Res. 2027;19(2):656-66.

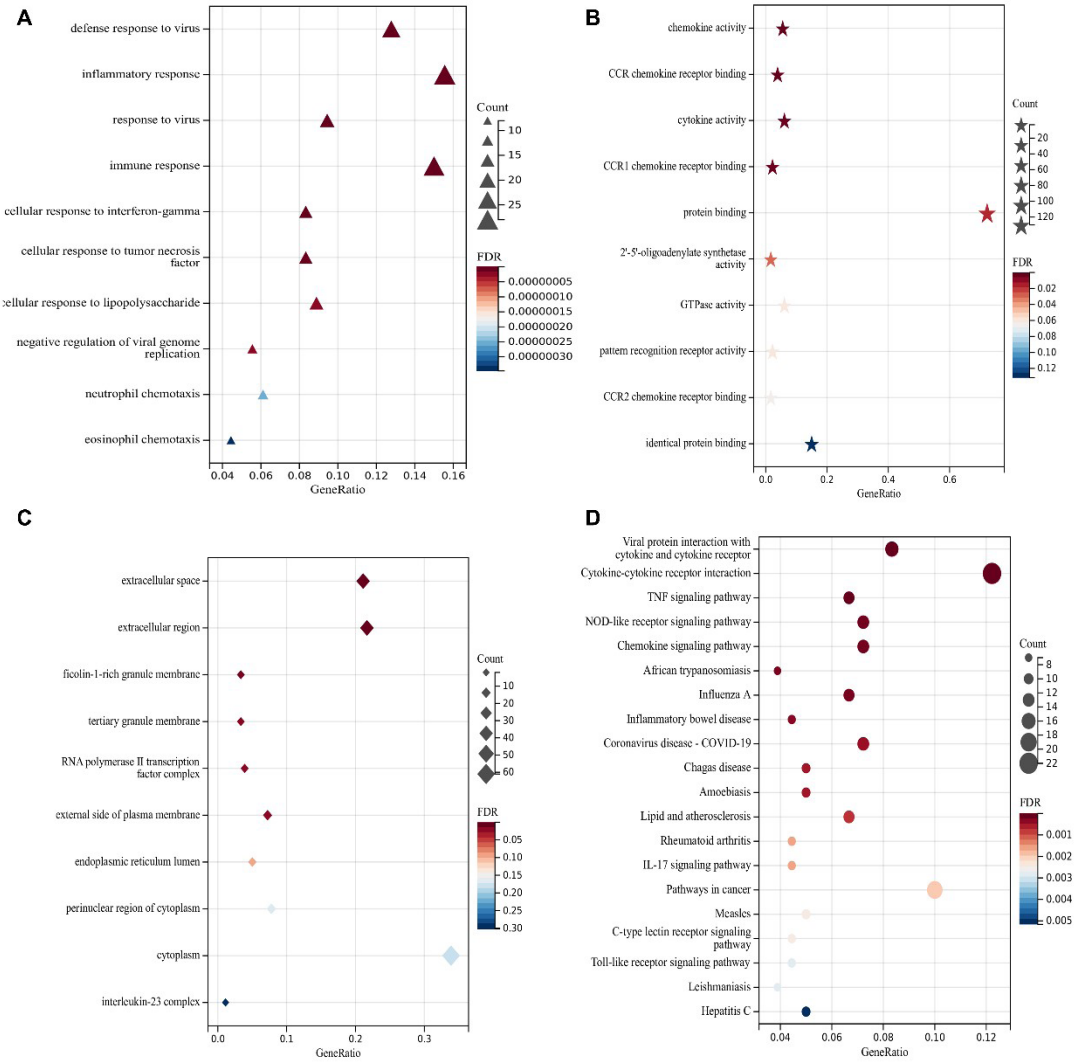


Figure S1: Functional annotation and enriched pathways associated with intersecting DEGs. (A) Biological Processes (BPs), (B) Molecular Functions (MFs), and (C) Cellular Components (CCs) identified via GO enrichment analysis. The bubble size corresponds to gene count and color intensity reflects P-value magnitude. (D) Top 20 KEGG pathways enriched among intersecting 180 DEGs. Visualization of bubble chart was performed using the DAVID platform.

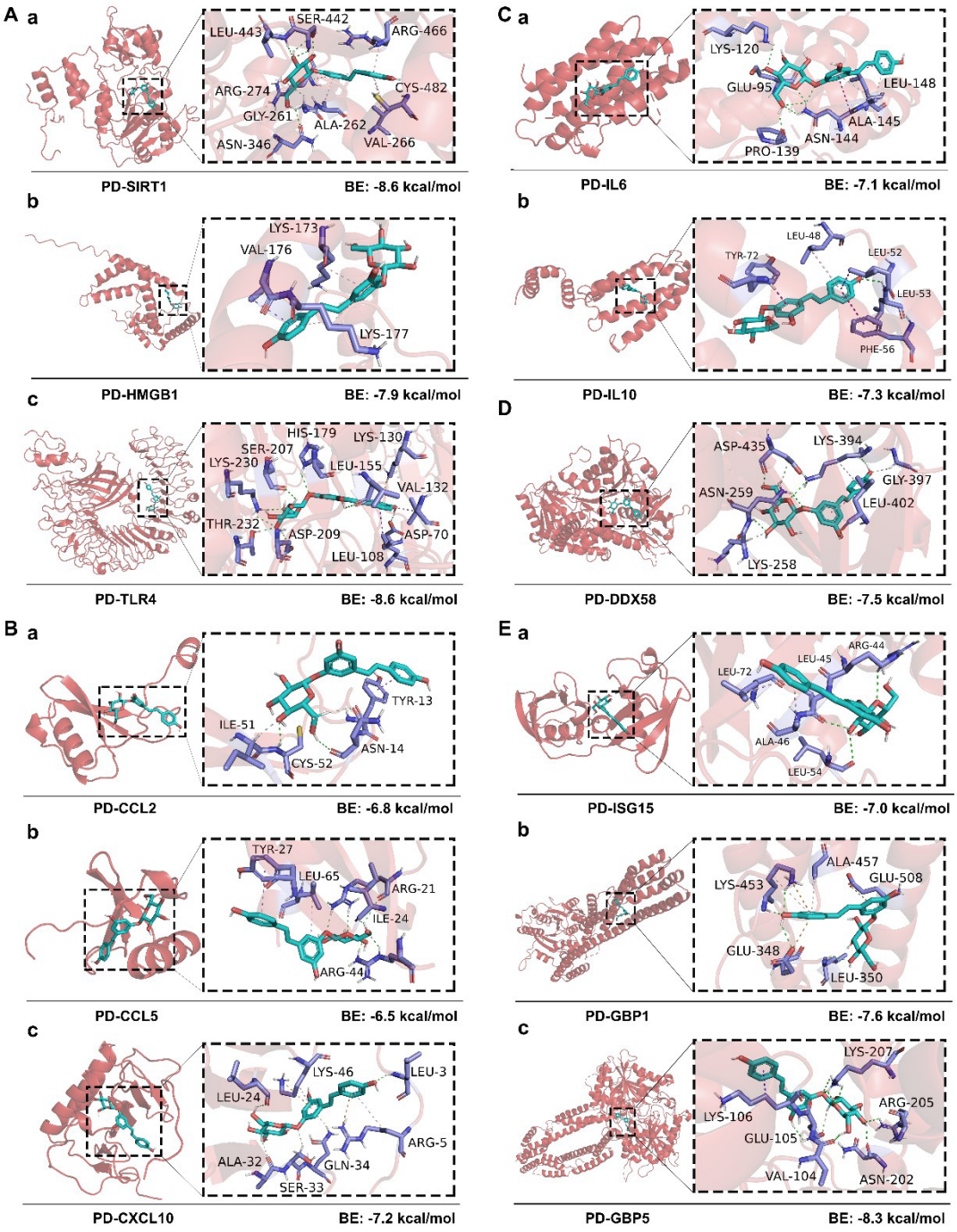


Figure S2: Three-dimensional molecular docking patterns of PD with hub genes. (A) Key factors of the signaling pathway, (a) SIRT1, (b) HMGB1, (c)TLR4. (B) Chemokines: (a) CCL2, (b) CCL5, (c) CXCL10. (C) Inflammatory cytokine: (a) IL- 6, (b) IL-10. (D) DDX58. (E) Interferon-stimulated factors: (a)ISG15, (b) GBP1, (c) GBP5.

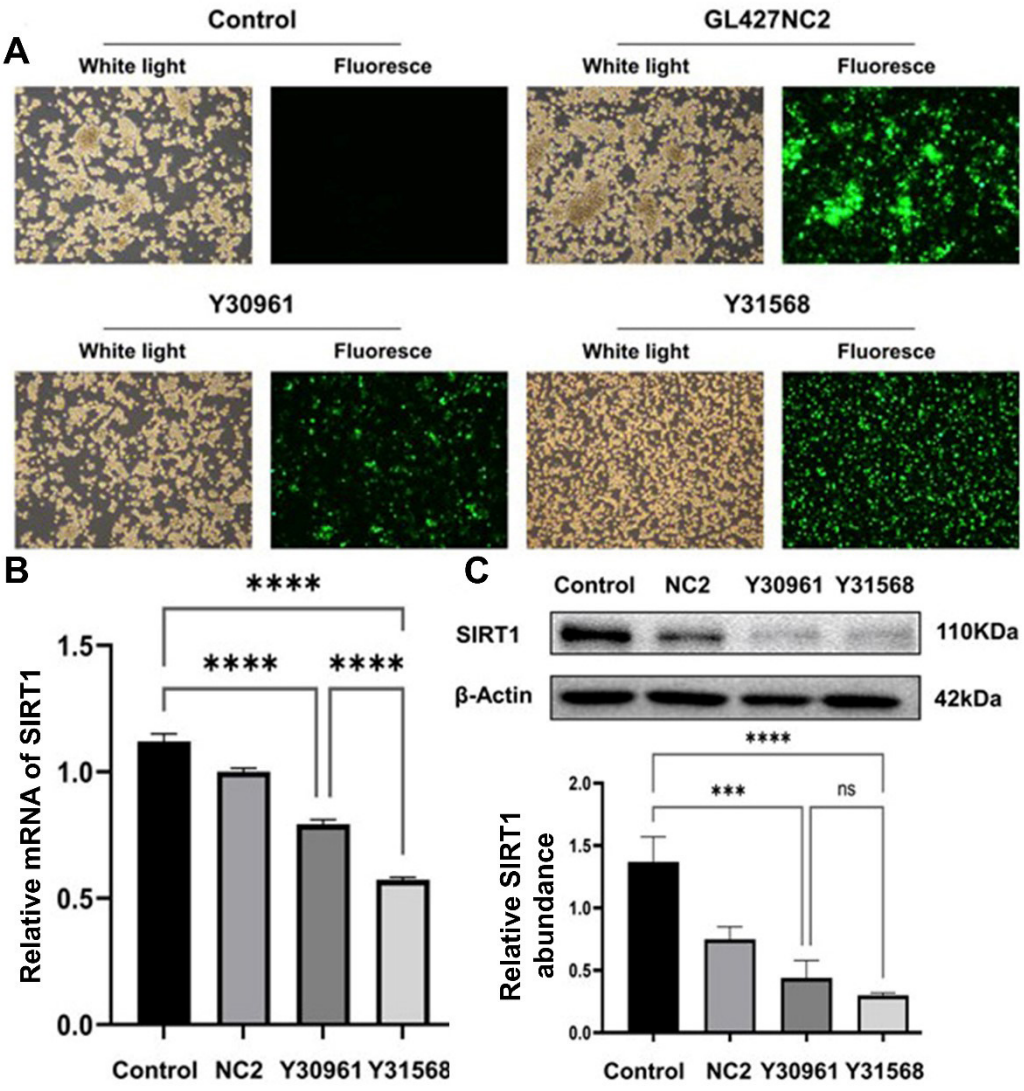
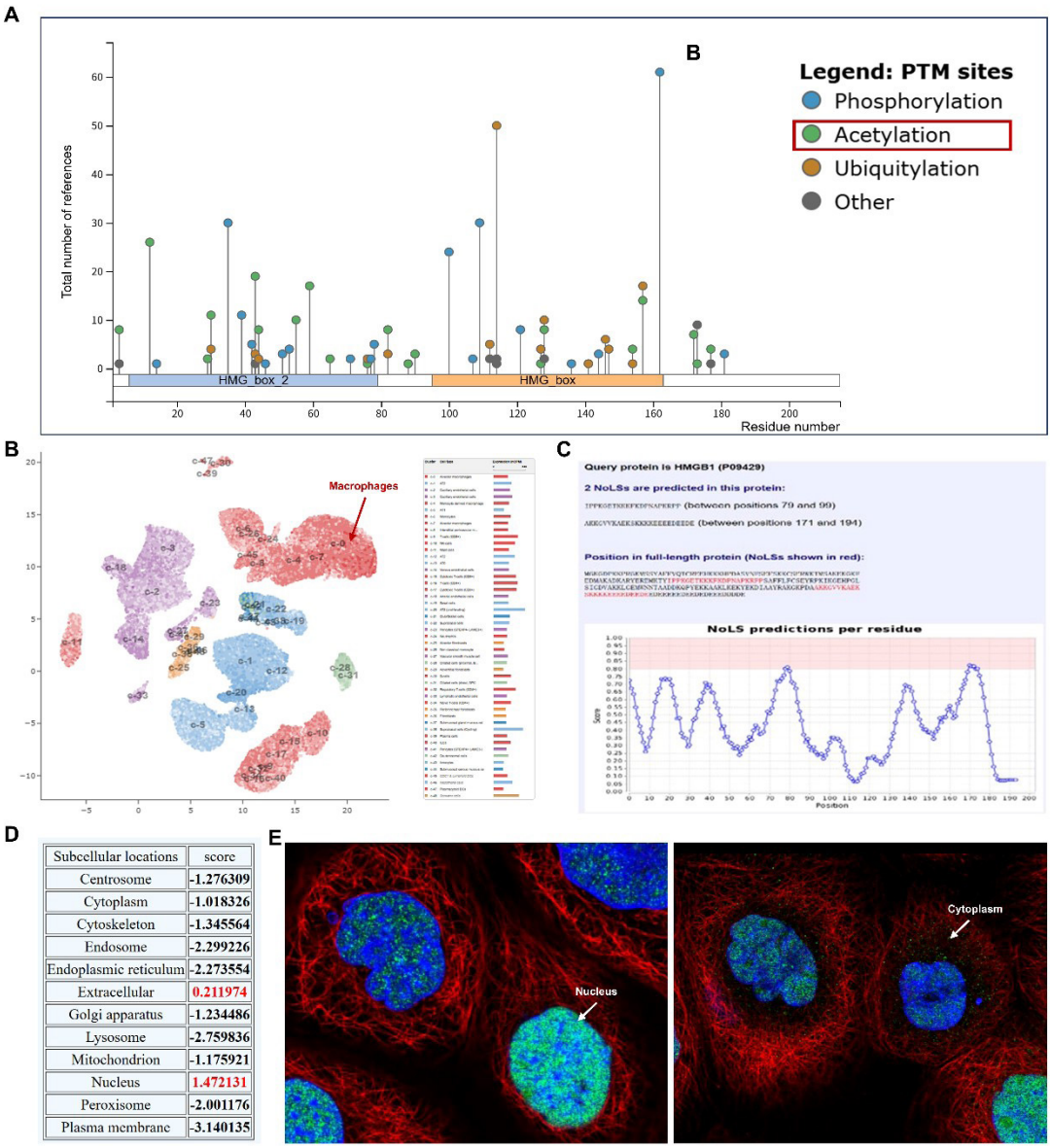


Figure S3: SIRT1-knockdown NR8383 cells were constructed. (A) GFP expression in NR8383 cells at 72 hr post-transduction. A significantly higher number of GFP-positive cells were found in the empty vector control groups and the SIRT1 knockdown group. (B) The SIRT1 expression results by qPCR showed that the use of Y31568 was the most effective method for SIRT1 knockdown in NR8383 cells. (C) Western blot analysis of SIRT1. All data are expressed as mean ± SD, ***p<0.001, ****p<0.0001, ns not significant.



Subcellular locations	score
Centrosome	-1.276309
Cytoplasm	-1.018326
Cytoskeleton	-1.345564
Endosome	-2.299226
Endoplasmic reticulum	-2.273554
Extracellular	0.211974
Golgi apparatus	-1.234486
Lysosome	-2.759836
Mitochondrion	-1.175921
Nucleus	1.472131
Peroxisome	-2.001176
Plasma membrane	-3.140135

Figure S4: Bioinformatics prediction of SIRT1-mediated deacetylation of HMGB1. (A) Prediction of HMGB1 acetylation sites using the PhosphoSitePlus. (B) Higher HMGB1 expression in macrophages was observed based on HPA datasets. (C) NoLSs prediction returned by NoD and the full-length protein sequence is displayed with the predicted NoLSs shown in red (D) The Subcellular localization score of HMGB1 using Cell-Ploc 3.0. (E) The localization analysis of HMGB1 (green) in the nucleus and cytoplasm in HPA datasets.

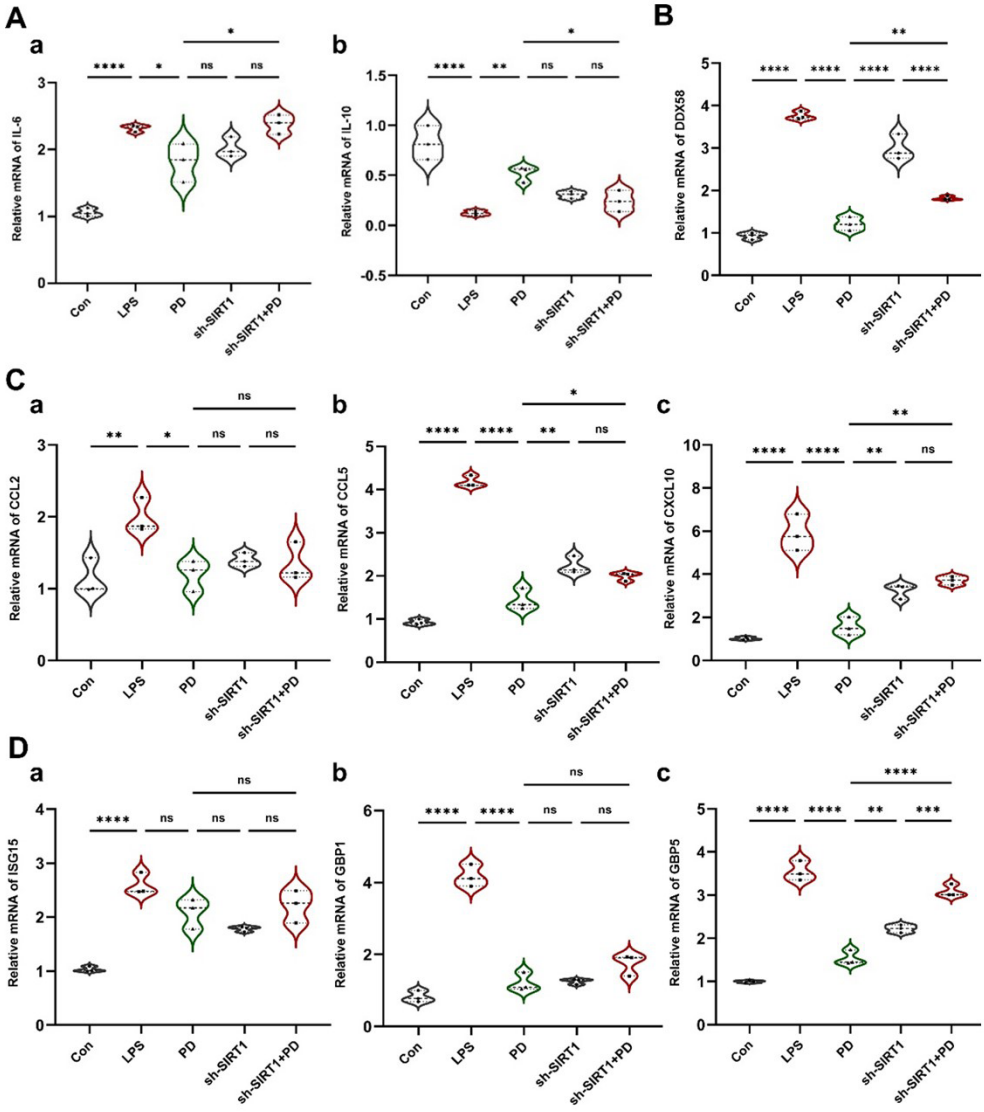


Figure S5: SIRT1-Knockdown influenced hub genes expression. (A) The mRNA ex-pression of IL-6 (a) and IL-10 (b) in NR8383 cells. (B) DDX58. (C) Chemokines: (a) CCL2, (b) CCL5, (c) CXCL10. (D) Interferon-stimulated factors: (a)ISG15, (b) GBP1, (c) GBP5. All data are expressed as mean values ± SD *p<0.05, **p<0.01, ***p<0.001, ****p<0.0001, ns not significant.